Modelling, Measurement and Control B
Vol. 88, No. 2-4, December, 2019, pp. 73-78
Journal homepage: http://iieta.org/journals/mmc_a

A Study on MHD Nanofluid Flow and Heat Transfer with Convective Surface Temperature and Concentration

K. Swain

Department of Mathematics, Gandhi Institute for Technology, Bhubaneswar 752054, India

Corresponding Author Email: kharabela1983@gmail.com

https://doi.org/10.18280/mmc_b.882-405

Received: 2 May 2019
Accepted: 26 August 2019

Keywords:
MHD, stretching sheet, nanofluid, thermal radiation, chemical reaction

ABSTRACT

An analysis has been carried out on MHD nanofluid flow over a stretching sheet embedded in a porous medium taking into account the first order chemical reaction. The uniform heat source/sink and thermal radiation affecting thermal energy distribution in the flow domain under convective heat and mass fluxes are also considered. The highly non-linear partial differential equations are transformed into ordinary differential equations with the help of similarity transformations. Numerical solutions for the governing momentum, energy and concentration equations are given. The physical significance of pertinent parameters on velocity, temperature and concentration as well as skin friction, rate of heat and mass transfer are shown in figures and tables. It is found that the power-law index, Brownian motion and thermophoresis parameters enhance the temperature distribution of the fluid. Higher Schmidt number i.e. heavier diffusing species reduces the solutal boundary layer thickness.

1. INTRODUCTION

Magnetohydrodynamics (MHD) nanofluid flow on a stretching sheet is of great interest in the field of engineering and technology especially extrusion of polymer sheet from expire, aerodynamic extrusion of plastic sheets, geothermal systems etc. Swain et al. [1] have studied the MHD heat and mass transfer on stretching sheet with variable viscosity as well as thermal conductivity. The thermo-diffusion has also been taken care of. Pattanaik et al. [2] have examined the MHD flow of an exponentially accelerated inclined plate in porous medium. The numerical solution of MHD flow over permeable stretching porous plate was studied by Mishra et al. [3]. Nayak [4] analyzed the effect of chemical reaction on MHD flow over a stretched vertical permeable surface with thermal radiation, heat source/sink. Das et al. [5] have considered the free convection flow of an elastic-viscous fluid past a vertical porous plate in a porous medium.

To develop the energy efficiency of heat transfer fluid, thermal conductivity plays an important role. The novelty of nanofluids offer fascinating heat transfer characteristics compared to conventional heat transfer fluids. Nanofluid is a combination of simple fluid and nanometer-sized particles (called nanoparticles) suspended uniformly in the fluid. There are many diverse applications of nanofluids such as biomedicines, nuclear reactors, refrigeration etc. Daniel [6] studied the boundary layer slip flow of nanofluid of a stretching sheet embedded in porous medium by using homotopy analysis method. Nield and Kuzentsov [7] discussed the thermal instability in a porous medium saturated by a nanofluid using the Buongiorno model. Swain et al. [8] have examined the inclusion of Joule heating, viscous dissipation, thermal radiation and non-uniform heat source on MHD Williamson nanofluid through porous medium. Khan and Pop [9] have studied nanofluid flow on a stretching surface. Makinde et al. [10] have analyzed the combined effects of Brownian motion and thermophoresis on stagnation point flow of nanofluid over a stretching sheet. Rout and Mishra [11] have studied MHD nanofluid flow over stretching sheet with or without slip. Ahmmed and Biswas [12] have examined the effects of thermal radiation and chemical reaction on MHD nanofluid flow through a vertical plate. Swain et al. [13] have studied the MHD flow of viscoelastic nanofluid over a stretching sheet with heat source/sink and chemical reaction.

The power-law model is an appropriate model to study characteristics of non-Newtonian fluids. This model usually defines the shear thinning/thickening of the fluid. Kavitha and Naikoti [14] have numerically studied the effects of viscous dissipation and suction/injection on MHD nanofluid flow over a permeable flat plate. Aziz and Jamshed [15] have analyzed the unsteady MHD slip flow of power-law nanofluid over a porous stretching sheet. Madhu and Kishan [16] have studied the mixed convection of non-Newtonian nanofluid obeying power-law model with power-law temperature and variable density.

In the present study we investigate a steady two dimensional boundary layer flow of an electrical conducting power-law nanofluid over a stretching sheet embedded in porous medium under the influence of transverse magnetic field and thermal slip as well as solutal slip. The impacts of thermal radiation, volumetric heat source/sink and chemical reaction parameter are also studied. The computations are carried out by using Runge-Kutta method along with shooting technique.

2. MATHEMATICAL FORMULATION

Consider the two dimensional steady incompressible MHD power-law nanofluid on a non-conducting stretching sheet y=0

embedded in porous medium. The flow of fluid is confined in the region y>0. The velocity, temperature and concentration of the stretching sheet are $u_w(x) = U_0 x^n$ (n being the power-law index), T_f and C_f respectively. A magnetic field $B = B_0 x^{\frac{n-1}{2}}$ is applied normal to the sheet. Further, the fluid assumed to be slightly conducting, the magnetic Reynolds number is much less than unity and hence the induced magnetic field is negligible. The coordinate system describing the flow model is given in Figure 1.

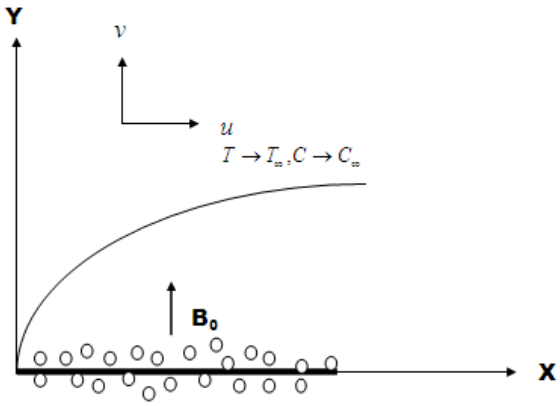

Figure 1. Flow geometry and coordinate system

The governing equations for the nanofluid can be written in Cartesian coordinates following Hayat et al. [17] with boundary conditions are given by

$$\frac{\partial u}{\partial x}+\frac{\partial v}{\partial y}=0 \tag{1}$$

$$\rho\left(u\frac{\partial u}{\partial x}+v\frac{\partial u}{\partial y}\right)=\mu\frac{\partial^2 u}{\partial y^2}-\sigma B_0^2 u-\frac{\mu}{Kp^*}u \tag{2}$$

$$u\frac{\partial T}{\partial x}+v\frac{\partial T}{\partial y}=\alpha\frac{\partial^2 T}{\partial y^2}+\tau\left[D_B\frac{\partial C}{\partial y}\frac{\partial T}{\partial y}+\frac{D_T}{T_\infty}\left(\frac{\partial T}{\partial y}\right)^2\right]-\frac{1}{(\rho C)_f}\frac{\partial q_r}{\partial y}+\frac{Q_0}{(\rho C)_f}(T-T_\infty) \tag{3}$$

$$u\frac{\partial C}{\partial x}+v\frac{\partial C}{\partial y}=D_B\frac{\partial^2 C}{\partial y^2}+\frac{D_T}{T_\infty}\frac{\partial^2 T}{\partial y^2}-k_c\left(C-C_\infty\right) \tag{4}$$

where, u and v are velocity components in the x and y directions, T the temperature, C the nanoparticle volume fraction, k the thermal conductivity, σ the electrical conductivity of the fluid, ρ is the density, $\tau=\frac{(\rho C)_p}{(\rho C)_f}$ is the ratio of effective heat capacity of the nanoparticle material and heat capacity of the fluid, k_c the rate of chemical reaction, D_B and D_T are the Brownian and thermophoresis diffusion coefficients respectively.

$$\left.\begin{aligned}&u=u_w(x)=U_0x^n, v=0,\ -k\frac{\partial T}{\partial y}=h_f\left(T_f-T\right),\ -D_m\frac{\partial C}{\partial y}=k_m\left(C_f-C\right)\ at\ y=0\\&u=0, v=0,\ T=T_\infty,\ C=C_\infty\ as\ y\to\infty\end{aligned}\right\} \tag{5}$$

We introduce the following similarity transformations

$$\left.\begin{aligned}&u=U_0x^n f'(\eta), v=-\sqrt{\frac{\upsilon_f U_0(n+1)}{2}}x^{\frac{n-1}{2}}\left\{f(\eta)+\frac{n-1}{n+1}\eta f'(\eta)\right\}\\&\eta=y\sqrt{\frac{U_0(n+1)}{2\upsilon_f}}x^{\frac{n-1}{2}}, \theta(\eta)=\frac{T-T_\infty}{T_f-T_\infty}, \phi(\eta)=\frac{C-C_f}{C_f-C_\infty}\end{aligned}\right\} \tag{6}$$

Using Eq. (6), the equations (2)-(4) reduce to

$$f'''+ff''-\frac{2n}{n+1}\left(f'\right)^2-\left(M+\frac{1}{Kp}\right)f'=0 \tag{7}$$

$$\left(1+R\right)\theta''+\Pr\left[f\theta'+Nb\theta'\phi'+Nt\left(\theta'\right)^2+Q\theta\right]=0 \tag{8}$$

$$\phi''+Scf\phi'+\frac{Nt}{Nb}\theta''-\gamma Sc\phi=0 \tag{9}$$

The non-dimensional boundary conditions (6) are

$$\left.\begin{aligned}&f(0)=0, f'(0)=1, \theta'(0)=-Bi_t\left[1-\theta(0)\right],\ \phi'(0)=-Bi_c\left[1-\phi(0)\right]\\&f'(\infty)=0,\ \theta(\infty)=0,\ \phi(\infty)=0\end{aligned}\right\} \tag{10}$$

where, non-dimensional variables and parameters are

$$M=\frac{2\sigma B_0^2}{\rho_f U_0(n+1)}, Kp=\frac{Kp^* a}{\upsilon}, \Pr=\frac{\upsilon_f}{\alpha}, Sc=\frac{\upsilon}{D_B}, Bi_c=\frac{k_m}{D_m x^{\frac{n-1}{2}}}\sqrt{\frac{2\upsilon_f}{U_0(n+1)}}$$

$$Nb=\frac{\tau D_B\left(C_\infty-C_f\right)}{\upsilon}, Nt=\frac{\tau D_T\left(T_\infty-T_f\right)}{\upsilon T_\infty}, \gamma=\frac{2}{n+1}\frac{k_c}{U_0x^{n-1}}, Bi_t=\frac{h_f}{k_f x^{\frac{n-1}{2}}}\sqrt{\frac{2\upsilon_f}{U_0(n+1)}}$$

The shearing stress, surface heat flux and surface mass flux are given by

$$\tau_w=\mu\left(\frac{\partial u}{\partial y}\right)_{y=0}, q_w=-k\left(\frac{\partial T}{\partial y}\right)_{y=0}+\left(q_r\right)_{y=0}, q_m=-D_B\left(\frac{\partial C}{\partial y}\right)_{y=0}$$

The non dimensional shear stress coefficient $C_f=\frac{\tau_w}{\rho U_0^2 x^{2n}}$, local Nusselt number $Nu_x=\frac{-xq_w}{k(T_f-T_\infty)}$, local Sherwood number $Sh_x=\frac{-xq_m}{D_B(C_f-C_\infty)}$ are given by

$$\left.\begin{aligned} C_f\left(\mathrm{Re}_x\right)^{1/2} &= \left(-\sqrt{\frac{n+1}{2}}\right) f''(0) \\ Nu_x\left(\mathrm{Re}_x\right)^{-1/2} &= -\left(\sqrt{\frac{n+1}{2}}\right)(1+R)\,\theta'(0) \\ Sh_x\left(\mathrm{Re}_x\right)^{-1/2} &= -\left(\sqrt{\frac{n+1}{2}}\right)\phi'(0) \end{aligned}\right\} \qquad (11)$$

where, $Re_x = \frac{U_0 x^{\frac{n+1}{2}}}{\upsilon_f}$ is the local Reynolds number.

3. NUMERICAL SOLUTION

The coupled non-linear equations (7)-(9) with convective thermal and solutal boundary conditions are solved numerically using the fourth-order Runge-Kutta method with a shooting technique. For this study, we consider the step size 0.01, error tolerance10^{-4} and η_{max}. To check the accuracy of the numerical method, we have compared our results with those of Mahapatra [18] and Madhu and Kishan [16]. The results are found in excellent agreement and shown in Table 1. Further, it is seen that from Figure 2 that velocity profiles exhibit a good coincidence with Hayat et al. [17].

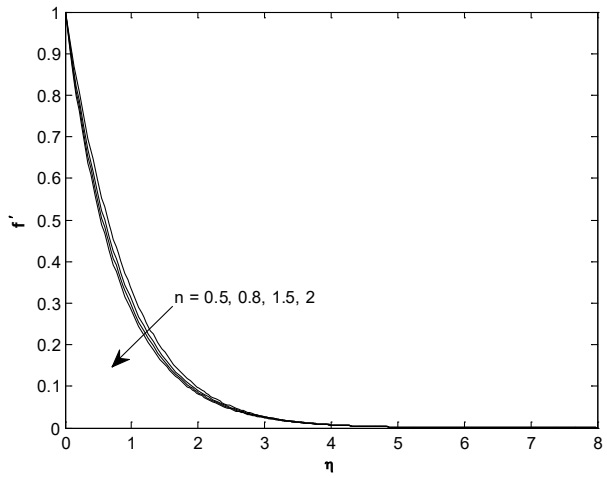

Figure 2. Comparison of velocity profile for *n* with Hayat et al. [17]

Table 1. Comparison of $f''(0)$ for various values of *M* at *n*=1

M	Mahapatra [18]	Madhu and Kishan [16]	Present Study
0.1	2.0175	2.01753	2.017856
0.5	2.1363	2.136374	2.135987
1.0	2.2491	2.249134	2.250046
1.5	2.3567	2.356684	2.356826
2.0	2.4597	2.459658	2.458915
3.0	2.6540	2.65378	2.654019
5.0	3.0058	3.00392	3.004687

4. RESULTS AND DISCUSSION

The numerical results achieved for velocity, temperature and concentration profiles for different values of pertinent parameters are illustrated through Figures 3-8. Computations have been carried out for $M = 0.5, Kp = 2, R = n = 1, Nb = 0.4, Nt = 0.3, Bi_t = Bi_c = 0.3, Q = \gamma = 0.1, \quad Pr = 1.3,$ and $Sc = 1.1$. Figure 3 displays the effect of magnetic parameter (M) and porosity parameter (Kp) on velocity distribution. The occurrence of magnetic field decreases the momentum boundary layer thickness. This is due to magnetic field produces a resistive force called Lorentz force which slows down the motion of the fluid. Therefore, an increase in *M* leads to decrease the velocity of the fluid. Further, porous matrix enhances the fluid flow. Figure 4 reveals the influence of power-law index (n) on velocity, temperature and concentration profiles. It is observed that velocity decreases with an increase in power-law index whereas opposite trend is seen in case of temperature profile. On the other hand, there is no significant effect of power-law index on concentration of nanofluid.

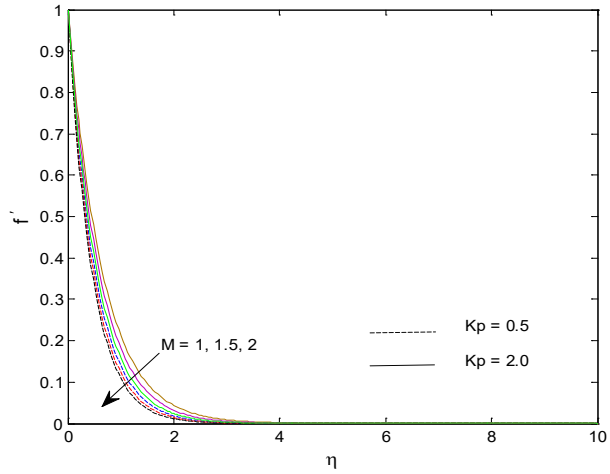

Figure 3. Effects of M and Kp on the velocity $f'(\eta)$ profile

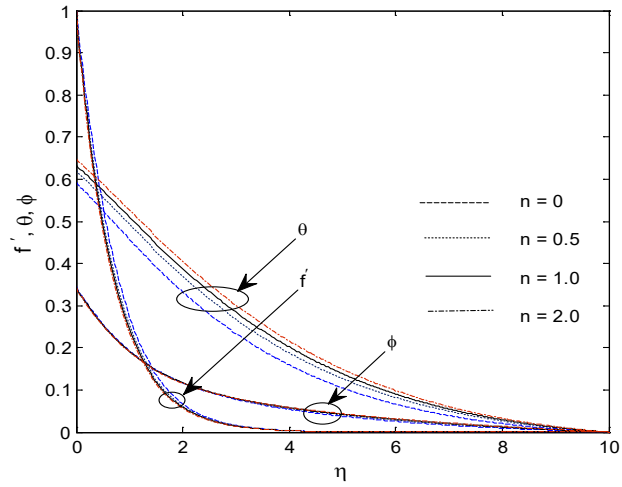

Figure 4. Effect of *n* on the velocity $f'(\eta)$, temperature $\theta(\eta)$ and concentration $\phi(\eta)$profiles

The effects of thermal radiation parameter (R) and heat source/sink (Q) are shown in Figure 5. Thermal radiation augments the thermal diffusivity of the nanofluid so that for higher values of *R*, heat will be added to the regime and temperature will be increased. It is noticed that, heat source parameter *Q(Q>0)* enhances the temperature of the nanofluid leading to an increase the thickness of the thermal boundary layer. But heat sink *Q(Q<0)* decreases the temperature profile. Figure 6 portrays the Brownian motion (Nb) and

thermophoresis parameter (Nt) on temperature and concentration profiles. It is noticed that temperature increases uniformly at all the layers as Nb and Nt increases. It is interesting to note that higher values of thermophoresis parameter increase the concentration but Brownian motion parameter decreases the concentration.

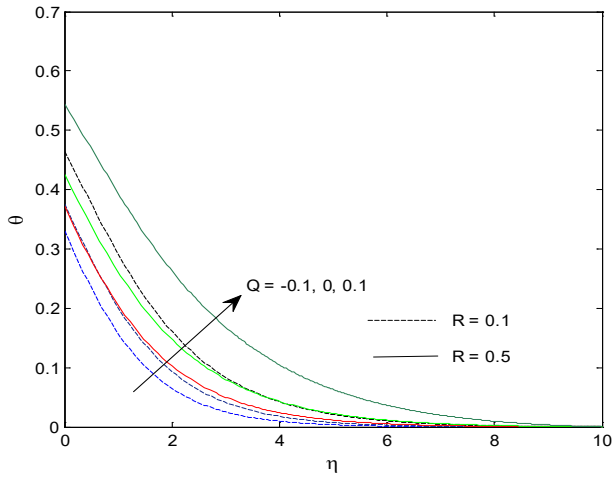

Figure 5. Effects of R and Q on the temperature$\theta(\eta)$profile

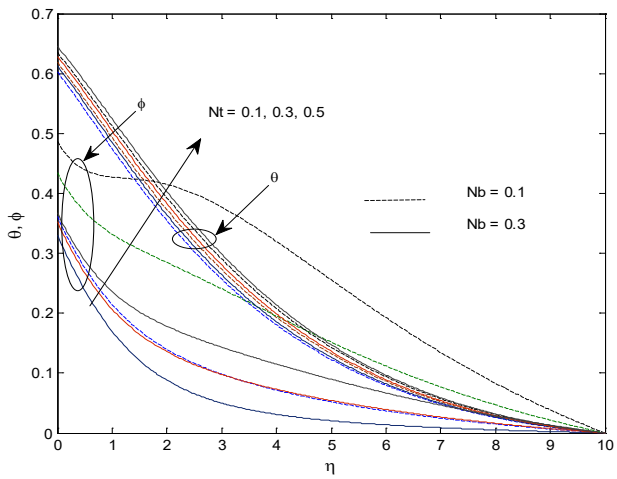

Figure 6. Effects of Nb and Nt on the temperature $\theta(\eta)$ and concentration $\phi(\eta)$ profiles

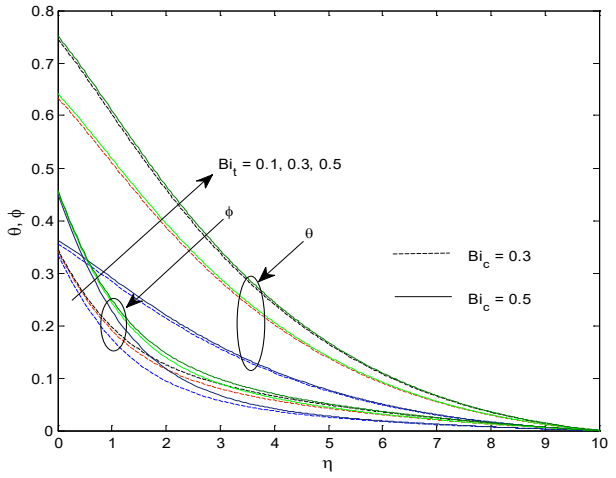

Figure 7. Effects of Bi_t and Bi_con the temperature $\theta(\eta)$and concentration $\phi(\eta)$ profiles

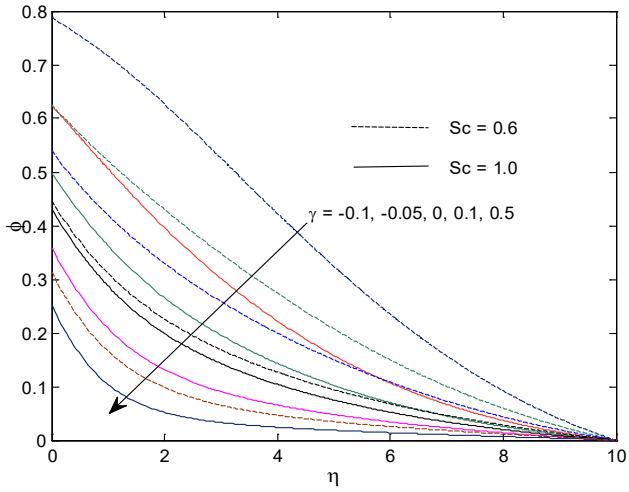

Figure 8. Effects of Sc and γ on the concentration $\phi(\eta)$ profile

Figure 7 is drawn to present the effects of thermal Biot number (Bi_t) and solutal Biot number (Bi_c) on temperature and concentration profiles. It is seen that both the parameters enhance the temperature and concentration profiles. Figure 8 depicts the influence of Schmidt number (Sc) and chemical reaction parameter *(γ)* on concentration profile. Higher values of Schmidt number i.e. heavier species reduce the concentration due to lower diffusion of mass. It is also noticed that destructive chemical reaction parameter *γ(γ>0)* decreases the concentration and constructive chemical reaction parameter *γ(γ<0)* increases concentration.

Table 2 exhibits the values of skin-friction coefficient $f''(0)$ Nusselt number $-\theta'(0)$ and Sherwood number $-\phi'(0)$. It is seen that skin friction at the wall increases as magnetic parameter and power-law index increase. But reverse tendency is observed due to porous matrix. It is interesting to note that Prandtl number, thermal radiation parameter and Schmidt number have no effects on skin friction. Further, it is noticed that increasing values of power-law index and radiation parameter increase the rate of heat transfer as well as mass transfer at the wall. Moreover, magnetic parameter, porous matrix, Prandtl number and Schmidt number have opposite effects on Nusselt number and Sherwood number.

Table 3 displays the values of Nusselt number $-\theta'(0)$ and Sherwood number $-\phi'(0)$. The heat and mass fluxes at the wall decrease with an increase in thermophoresis parameter (Nt). Brownian motion and solutal Biot number decrease the heat flux at the surface but adverse effect is observed in case of mass flux. Further, it is noticed that Nusselt number increases with increase in thermal Biot number while Sherwood number decreases. One interesting result is that the rate of heat transfer at the wall decreases significantly with an increase in heat source parameter *Q(Q)>0* where as the adverse effect is observed in presence of heat sink *Q(Q<0)*. Further, heat source increases the Sherwood number but heat sink reduces it. On careful observation, it is seen that for destructive chemical reaction parameter *γ(γ>0)*, the Sherwood number increases with an increase in γ but decreases with an increase in constructive chemical reaction parameter *γ(γ<0)*. Moreover, in an exothermic reaction, the rate of heat transfer at the wall increases while in endothermic reaction it decreases.

Table 2. Computation of skin friction coefficients, Nusselt number and Sherwood number when $Q=\gamma=0.1$, $Nb=Nt=0.5$, $Bi_t=Bi_c=0.3$

M	***Kp***	***n***	***Pr***	***R***	***Sc***	***f''(0)***	$-\theta'(0)$	$-\phi'(0)$
0.1	2	1	1	0.1	0.6	1.26491	0.15753	0.15135
0.5						1.41421	0.14138	0.15425
	1					1.58114	0.11792	0.16081
		1.5				1.81350	0.12811	0.18098
		2				2.01933	0.13759	0.19915
			2			2.01933	0.22279	0.16428
			7			2.01933	0.29389	0.13349
				0.5		2.01933	0.38526	0.13858
				1		2.01933	0.48907	0.14458
					1	2.01933	0.48296	0.19401
					2	2.01933	0.48016	0.24885

Table 3. Computation of Nusselt number and Sherwood number when $M=0.5$, $Kp=2$, $Sc=0.6$ $n=Pr=R=1$

Nb	***Nt***	Bi_t	Bi_c	γ	***Q***	$-\theta'(0)$	$-\phi'(0)$
0.1	0.1	0.1	0.1	0.1	0.1	0.12133	0.07796
0.5						0.11950	0.08073
0.9						0.11763	0.08104
	0.3					0.11580	0.08051
	0.5					0.11388	0.08011
		0.3				0.17576	0.07979
		0.5				0.19561	0.07977
			0.3			0.17832	0.17627
			0.5			0.16842	0.23250
				0.2		0.17125	0.25450
				0.5		0.17644	0.29177
				-0.1		0.15421	0.11414
				-0.2		0.05531	0.53456
				0.2	0	0.32378	0.23535
					-0.1	0.39459	0.22598
					-0.2	0.44009	0.21971

5. CONCLUSION

MHD flow and heat transfer of nanofluid over a stretching sheet embedded in porous medium with heat source/sink, thermal radiation, chemical reaction and convective heat and mass fluxes are studied. The governing PDEs are transformed into a system of coupled non-linear ODEs by using similarity transformations. The effects of various thermo-physical parameters governing the flow problem on velocity, temperature and concentration are represented through graphs and tables and also discussed in details.

The following conclusions are drawn:

(1) Velocity profile decreases with an increase in magnetic number and power-law index.

(2) Power-law index, Brownian motion and thermophoresis parameters enhance the temperature profile of the flow.

(3) Thermal radiation parameter favours the growth of thermal boundary layer.

(4) Heat source parameter enhances the temperature profile whereas heat sink reduces it.

(5) Both thermal and solutal Biot numbers enhance the temperature as well as concentration profiles.

(6) The presence of heavier species in the flow field (higher *Sc*) decreases the concentration in the boundary layer.

(7) Brownian motion and thermophoresis parameters have opposite effects on concentration of nanoparticles.

(8) Destructive chemical reaction parameter decreases the concentration profile whereas constructive chemical reaction parameter increases the concentration profile.

REFERENCES

[1] Swain, K., Parida, S.K., Dash, G.C. (2017). MHD heat and mass transfer on stretching sheet with variable fluid properties in porous medium. AMSE-Journals, Modelling B, 86(3): 706-726.

[2] Pattanaik, J.R., Dash, G.C., Singh, S. (2017). Radiation and mass transfer effects on MHD flow through porous medium past an exponentially accelerated inclined plate with variable temperature. Ain Shams Engineering Journal. 8(1): 67-75. https://doi.org/10.1016/j.asej.2015.08.014

[3] Mishra, S.R., Nayak, B., Sharma, R.P. (2017). MHD stagnation-point flow past over a stretching sheet in the presence of non-Darcy porous medium and heat source/sink. Defect and Diffusion Forum, 374: 92-105.

[4] Nayak, M.K. (2016). Steady MHD flow and heat transfer on a stretched vertical permeable surface in presence of heat generation/absorption, thermal radiation and chemical reaction. AMSE Journals, Modelling, Measurement and Control B, 85(1): 91-104.

[5] Das, S.S., Panda, J.P., Dash, G.C. (2004). Free convection flow and mass transfer of an elastic viscous fluid past an infinite vertical porous plate in a rotating porous medium. AMSE Journals Modelling, Measurement and Control B, 73: 37-52.

[6] Daniel, Y.S. (2015). Presence of heat generation/absorption on boundary layer slip flow of nanofluid over a porous stretching sheet. American Journal of Heat and Mass Transfer, 2(1): 15-30. https://doi.org/10.7726/ajhmt.2015.1002

[7] Nield, D.A., Kuzentsov, A.V. (2009). Thermal instability in a porous medium layer saturated by a nanofluid. International Journal of Heat and Mass Transfer, 52: 5796-5801. https://doi.org/10.1016/j.ijheatmasstransfer.2009.07.023

[8] Swain, K., Parida, S.K., Dash, G.C. (2018). Effects of non-uniform heat source/sink and viscous dissipation on MHD boundary layer flow of Williamson nanofluid through porous medium. Defect and Diffusion Forum, 389: 110-127. https://doi.org/10.4028/www.scientific.net/DDF.389.110

[9] Khan, W.A., Pop, I. (2010). Boundary-layer flow of a nanofluid past a stretching sheet. International Journal of Heat and Mass Transfer, 53: 2477-2483. https://doi.org/10.1016/j.ijheatmasstransfer.2010.01.032

[10] Makinde, O.D., Khan, W.A., Khan, Z.H. (2013). Buoyancy effects on MHD stagnation point flow and heat transfer of a nanofluid past a convectively heated stretching/shrinking sheet. International Journal of Heat and Mass Transfer, 62: 526-533. https://doi.org/10.1016/j.ijheatmasstransfer.2013.03.049

[11] Rout, B.C., Mishra, S.R. (2018). Thermal energy transport on MHD nanofluid flow over a stretching surface: A comparative study. Engineering Science and Technology, an International Journal, 21: 60-69. https://doi.org/10.1016/j.jestch.2018.02.007

[12] Ahmmed, S.F., Biswas, R. (2018). Effects of radiation and chemical reaction on MHD unsteady heat and mass transfer of nanofluid flow through a vertical plate. Modelling, Measurement and Control B, 87(4): 213-220. https://doi.org/10.18280/mmc_b.870401

[13] Swain, K., Parida, S.K., Dash, G.C. (2018). MHD flow of viscoelastic nanofluid over a stretching sheet in a porous medium with heat source and chemical reaction. Annals of Chemistry- Materials Science, 42(1): 7-21.

[14] Kavitha, P., Kishan, N. (2019). MHD boundary layer flow of non-Newtonian power-law nanofluid with thermal radiation. Journal of Nanofluids, 8(1): 84-93.

[15] Aziz, A., Jamshed, W. (2018). Unsteady MHD slip flow of non Newtonian power-law nanofluid over a moving surface with temperature dependent thermal conductivity. American Institute of Mathematical Sciences, 11(4): 617-630.

[16] Madhu, M., Kishan, N. (2016). Finite element analysis of heat and mass transfer by MHD mixed convection stagnation-point flow of a non-Newtonian power-law nanofluid towards a stretching surface with radiation. Journal of Egyptian Mathematical Society, 24: 458-470. https://doi.org/10.1016/j.joems.2015.06.001

[17] Hayat, T., Rashid, M., Imtiaz, M., Alsaedi, A. (2015). Magnetohydrodynamic (MHD) stretched flow of nanofluid with power-law velocity and chemical reaction. AIP Advances, 5: 117121. https://doi.org/10.1063/1.4935649

[18] Mahapatra, T.R., Nandy, S.K., Gupta, A.S. (2009). Analytical solution of magnetohydrodynamic stagnation-point flow of a power-law fluid towards a stretching surface. Appl. Math. Comput, 215: 1696-1710. https://doi.org/10.1016/j.amc.2009.07.022

NOMENCLATURE

u, v	velocity components along the x and y axes respectively
D_B	Brownian diffusion coefficient
D_T	thermophoresis diffusion coefficient
T	nanofluid temperature
$(\rho C)_f$	heat capacity of the nanofluid
$(\rho C)_p$	effective heat capacity of nanoparticle
B	magnetic field strength
Kp^*	permeability of the porous medium
k_c	rate of chemical reaction
C	volumetric volume fraction
T_w	temperature of the nanofluid near wall
T_∞	free stream temperature of the nanofluid
k	thermal conductivity
M	magnetic parameter
Bi_t	thermal Biot number
Bi_c	solutal Biot number
n	power-law index
Kp	permeability parameter
Pr	Prandtl number
Nb	Brownian motion parameter
Nt	thermophoresis parameter
Sc	Schmidt number

Greek symbols

η	similarity variable
θ	dimensionless temperature
$\emptyset$	dimensionless concentration
ρ	density of the nanofluid
α_m	nanofluid thermal diffusivity
υ	kinematic viscosity
τ	ratio between the effective heat capacity of the nanoparticle material and the fluid
γ	chemical reaction parameter